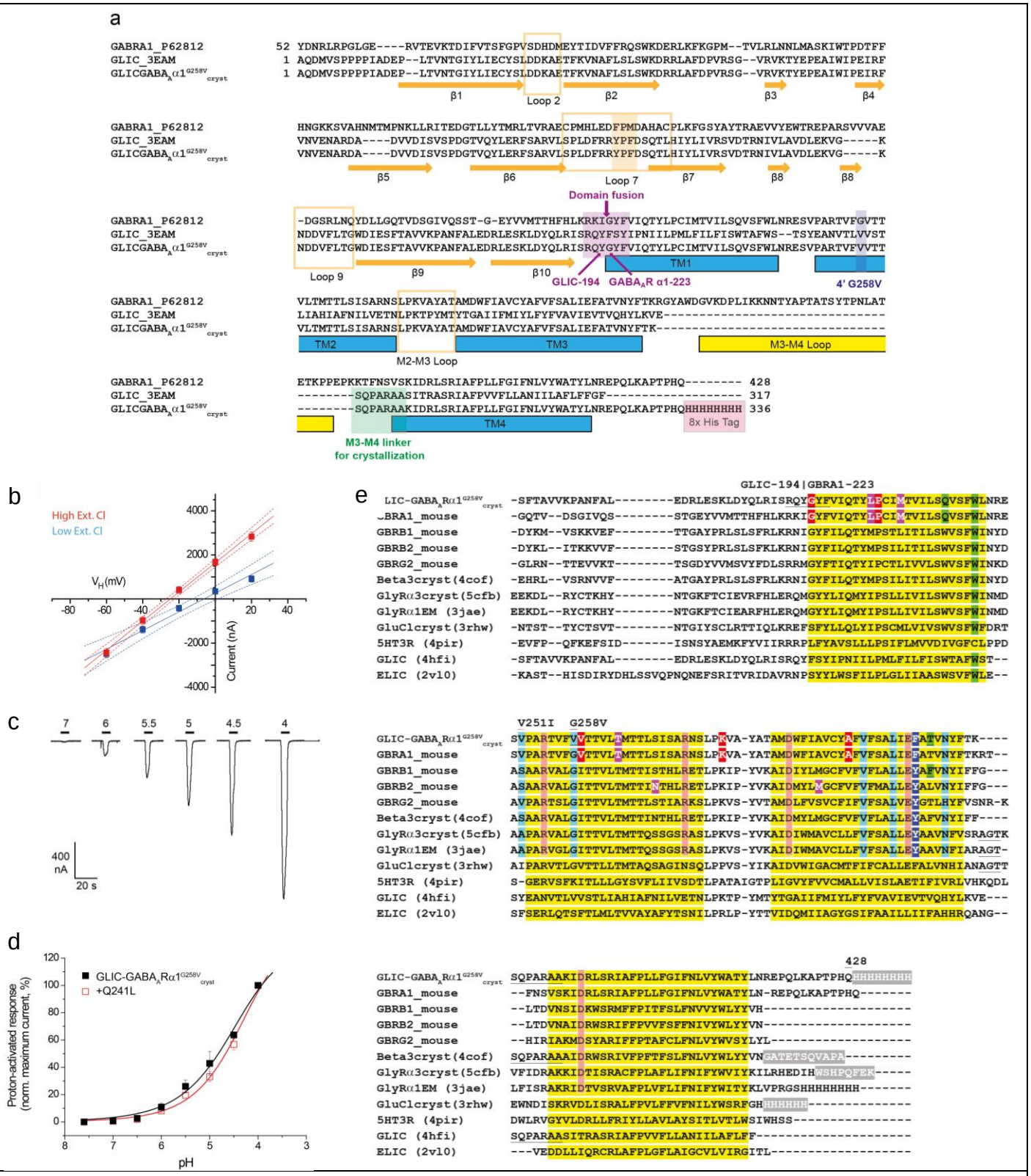


**Supplementary Figure 1**

GLIC-GABA$_A$Rα1$^{G258V}_{cryst}$: crystallization chimera, its functional characterization and TMD sequence alignment with pLGICs

(**a**) Sequence alignment for GLIC-$GABA_AR\alpha1^{G258V}_{cryst}$ with WT GLIC and $GABA_AR$ α1 subunits. The point of ECD-TMD fusion is highlighted. For clarity, numbering of residues in the chimera corresponds to the numbering of each parent protein: chimera numbering at the point of domain fusion and the start of the $GABA_AR$ TMD (M1) commences from residue 223. Truncation and replacement of the intracellular loop (residues 312 - 389 in M3-M4 linker) is highlighted in green and the octa-His purification tag is highlighted in pink. Secondary structure annotation of the ECD is based upon that observed for GLIC. (**b**) Current-voltage relationship for the chimera expressed in *Xenopus* oocytes determined using Ringer solution containing either 108 mM (red) or 27 mM (blue) external $Cl^-$. Isethionate ions were used as an impermeant $Cl^-$ ion replacement. The solid lines are linear regression fits to mean ± sem data with 95 % confidence intervals shown as dashed lines (n = 6 independent experiments for each). The predicted $E_{Cl}$ values from the Nernst equation were +2.8 and -34 mV for $[Cl^-]_o$ 27 and 108 mM, assuming an $[Cl^-]_i$ of 30 mM. The actual mean $E_{Cl}$ values are -5 and -26 mV (uncorrected for junction potentials which are <2 mV). This shift in $E_{Cl}$ on changing $[Cl^-]_o$ is broadly in accord with a $Cl^-$ selective channel. (**c**) Two-electrode voltage clamp proton concentration current responses of the chimera recorded at -60 mV over a range of extracellular pH conditions following expression in oocytes. Note the chimera is mostly inactive at neutral pH and efficiently gated by protons. (**d**) Proton concentration-response curves for the chimera, and the Q241L mutation expressed in *Xenopus* oocytes voltage clamped at -60 mV. Normalized mean (± sem) peak current responses to increasing proton concentrations were fitted to the Hill equation (see Methods) in order to determine the following $EC_{50}$ values: GLIC-$GABA_AR\alpha1^{G258V}_{cryst}$, pH 4.5 ± 0.11; +Q241L, pH 4.4 ± 0.12, n = 6, independent experiments for each. (**e**) The transmembrane domains of selected $GABA_AR$ subunits and various pLGICs (for which structures have been determined) were aligned using PROMALS3D. Accession codes for mouse GABA subunits are; α1 (P62813); β1 (P50571); β2 (P63137); γ2 (P22723). PDB ID numbers for the pLGICs are shown in parentheses, and the deposited sequences (typically reflecting purification constructs) were used in the alignment. The TMDs are highlighted in yellow. Residues mediating inhibitory pLGIC desensitization[10] are highlighted in pale-blue, and a conserved aromatic residue (Phe, Tyr) at the base of M3 (identified in the GABA β3 structure) in dark blue. Residues mediating the response to neurosteroids are highlighted in green. Residues identified in binding studies of general anaesthetics for $GABA_AR$ α1- and β2-subunits, are highlighted in purple. Residues associated with disease-related mutations in the α1 TMD are highlighted in red. Conserved residues which form salt-bridge interactions are highlighted in pink. C-terminal purification tags used in the crystallization constructs are highlighted in grey.

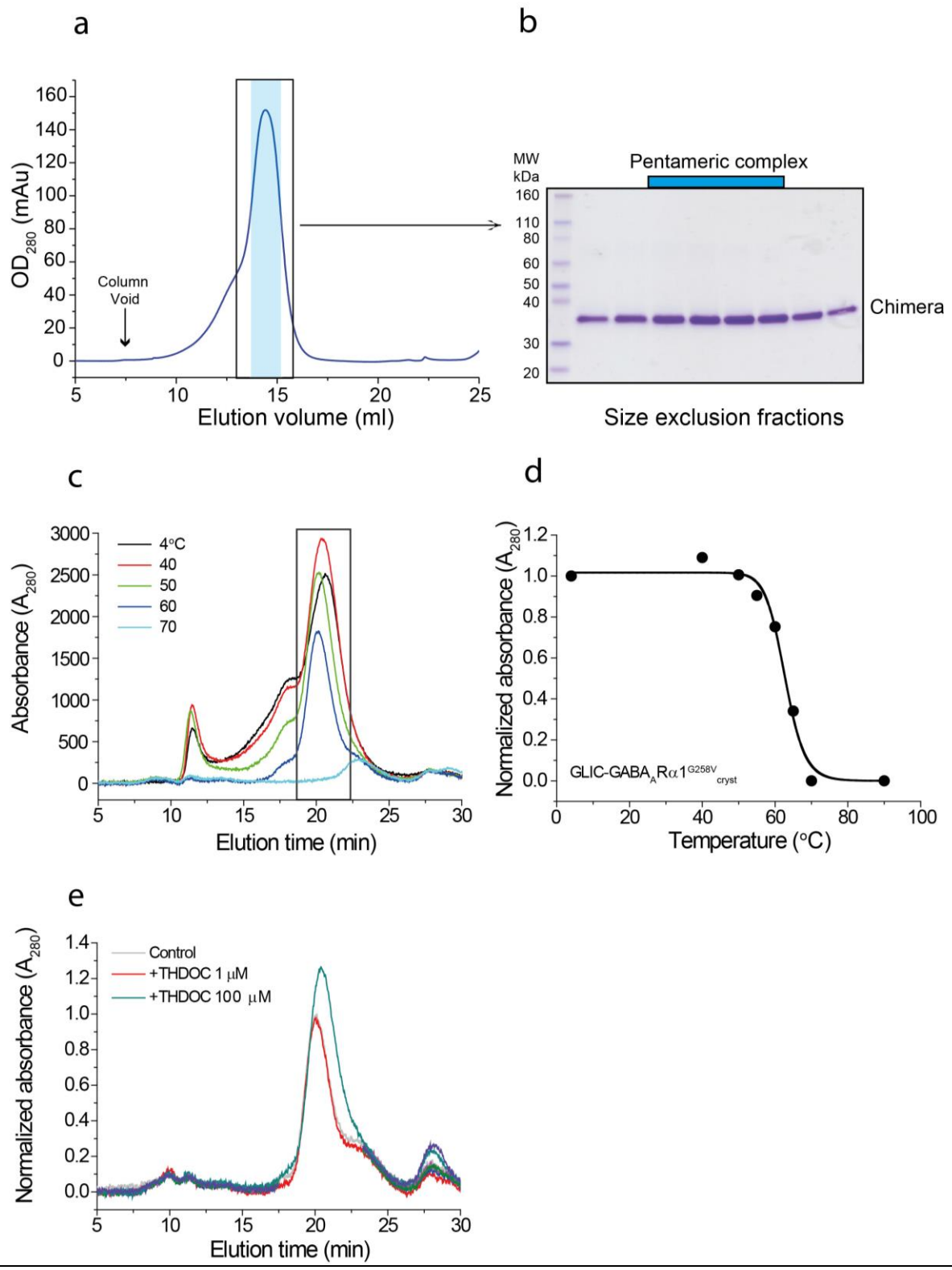


**Supplementary Figure 2**

Receptor chimera purification and crystallization

(**a**) Size exclusion chromatography (SEC) purification profile for the GLIC-$GABA_AR\alpha1^{G258V}_{cryst}$ receptor-detergent complex following isolation by immobilized metal ion affinity chromatography (IMAC). The major species elutes as a symmetrical peak (highlighted blue). (**b**) Material taken from the peak in (**a**) (boxed) migrates as a single band by SDS-PAGE indicative of an intact pentameric complex. **(c)** Representative SEC profiles of purified crystallization construct (following detergent solubilisation) after heating over the indicated range of temperatures for 1 hr. The peak intensity corresponding to the pentameric receptor (outlined by the box) was used for analysis. (**d**) Representative melting curve for the crystallization construct. The melting temperature ($T_m$ = 62 $^oC$) was calculated by fitting the data to a sigmoidal equation. **(e)** Representative SEC profiles for the crystallization construct in the presence of the indicated concentrations of THDOC and after heating at 62 °C for 1 hr. Incubation in 100 μM THDOC induced an approximate 25 % increase in thermal stability.

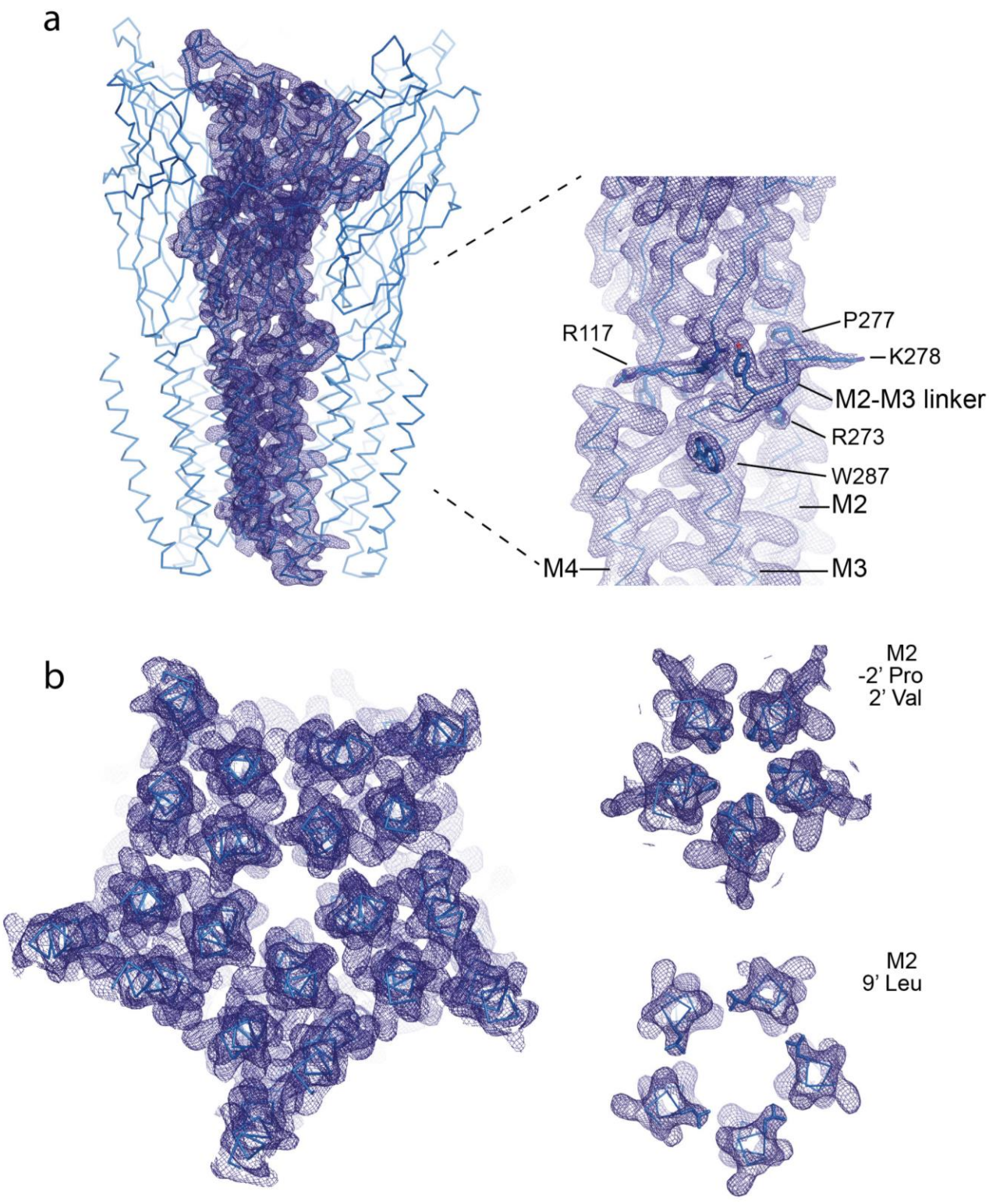


**Supplementary Figure 3**

Electron density maps for the *apo* form of the chimera

(**a**) The *apo* form of the chimera is shown in α-carbon trace representation and the sigma A-weighted $2F_o$-$F_c$ electron density map (dark blue; contoured at 1.2σ) is shown for a single subunit. (**b**) Electron density maps taken for transverse sections through the TMD (left), and (right) at the level of the selectivity filter (-2' Pro and 2' Val residues) and activation gate (9' Leu).

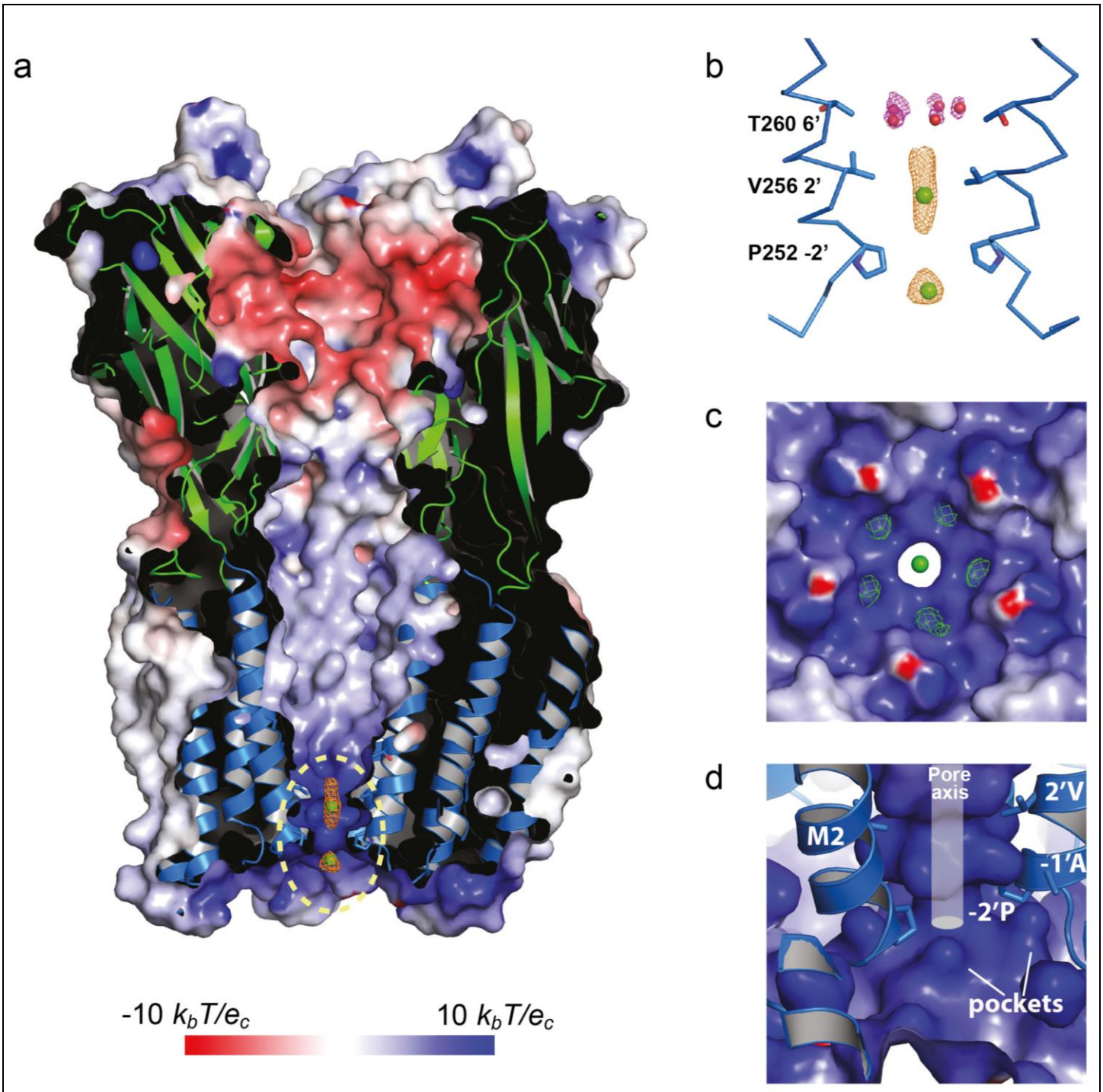


**Supplementary Figure 4**

Electrostatic surface potential map of the GLIC-GABA$_A$Rα1$^{G258V}_{cryst}$ channel and $Cl^-$ site

(**a**) Longitudinal cross-section through the chimera is shown, revealing the electrostatic surface potential along the ion-conducting pathway. A region of electropositive charge at the base of the ion channel is highlighted by a yellow oval and magnified in the right panels. Additional density at the intracellular portal of the ion channel (~6σ in $F_o$-$F_c$ maps) was modeled as a $Cl^-$ ion (green sphere; see panel **b** & **c**) with omit-style electron density (calculated in PHENIX; orange map) shown at 2σ. The $Cl^-$ is located along the five-fold

symmetry axis. (**b**) A self-stabilized pentameric arrangement of water molecules (red spheres) forms at the level of the 6' threonines, above two putative $Cl^-$ (green spheres) binding sites between 2' and -3' M2. $F_o$-$F_c$ omit densities are shown at 2σ for $Cl^-$ (orange map) and 1σ for water (magenta map). (**c**) Putative $Cl^-$ binding sites in electropositive pocket formed at the base of the channel by residues in M2 and M1-M2 loop (positive peaks in $F_o$-$F_c$ electron density maps shown as a green mesh, contoured at 4σ). (**d**) Pockets in (**c**) as viewed from within the helical bundle at the level of the ion selectivity filter (-2'/-1').

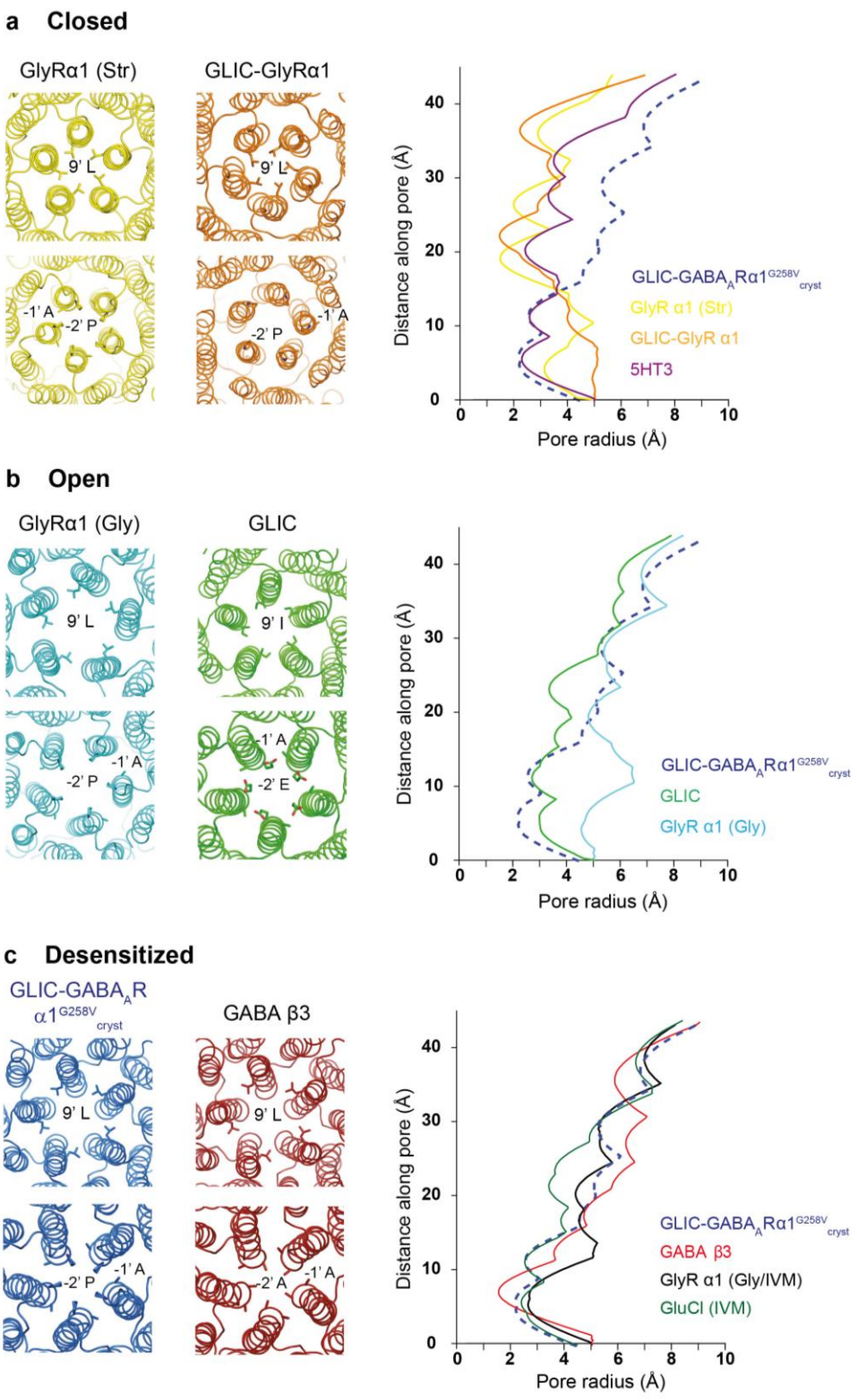


**Supplementary Figure 5**

Pore residues and ion channel profiles for GLIC-GABA$_A$Rα1$^{G258V}_{cryst}$ and pLGICs

Ribbon and stick-form plan views of the relative positions of residues in M2 α-helices that form the 9' activation gate (upper panels) and the 2' to -2' desensitization gate/ion selectivity filter (lower panels), for selected pLGIC structures (viewed from extracellular and intracellular sides, respectively). The pore-profiles for receptors are shown in the plots (right) with the profile of proton-bound GLIC-$GABA_AR\alpha1^{G258V}_{cryst}$ replicated (dashed blue line) for comparison. These have been separated into (**a**) Closed/Locally-closed states, (**b**) Open-states and (**c**) Desensitized/Partially-open states. Abbreviations: Str, Strychnine; Gly, Glycine; IVM, ivermectin.

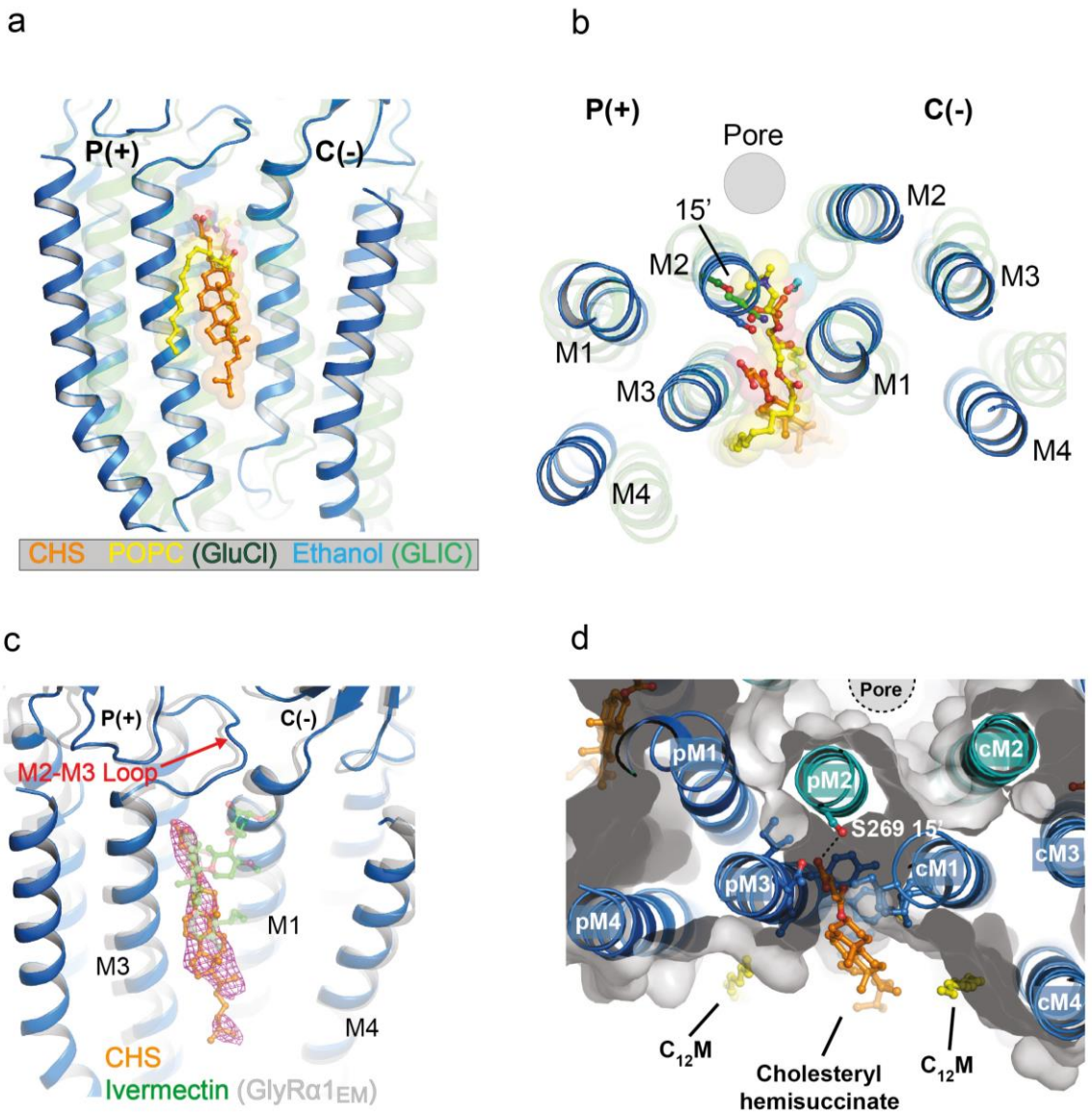


**Supplementary Figure 6**

Cholesteryl hemisuccinate binds to an interfacial site in GLIC-$GABA_AR\alpha1^{G258V}_{cryst}$

(**a**) Side-view of the chimera (in cartoon representation) at the interface between two subunits showing the location of bound cholesteryl hemisuccinate (CHS; stick form, orange). The location of CHS spatially overlaps with the binding sites previously identified in GLIC for the lipid POPC in GluCl (PDB ID: 4tnw)[39] and ethanol (PDB ID: 4hfe)[22]. (**b**) Plan view from (**a**) reveals the interfacial binding site for CHS, POPC and ethanol viewed from the extracellular side. (**c**) Structural superimposition of the chimera with GlyRα1 (grey cartoon) in complex with ivermectin (green stick-form; PDB ID: 3jaf) reveals overlapping binding sites for CHS (orange stick-form) and ivermectin. Omit density map for CHS (magenta) is contoured at 1σ. (**d**) Residues forming a hydrophobic belt around CHS are shown in stick-form. (Principal face: M2 – S269, M3 – A290, Y293, F297; Complementary face: M1 – I297, L231, M235). The hemisuccinate group on ring A of CHS protrudes into the subunit interface forming a polar contact with the 15' S269 in M2. Acyl chain of DDM detergent molecules ($C_{12}M$) is shown in yellow.

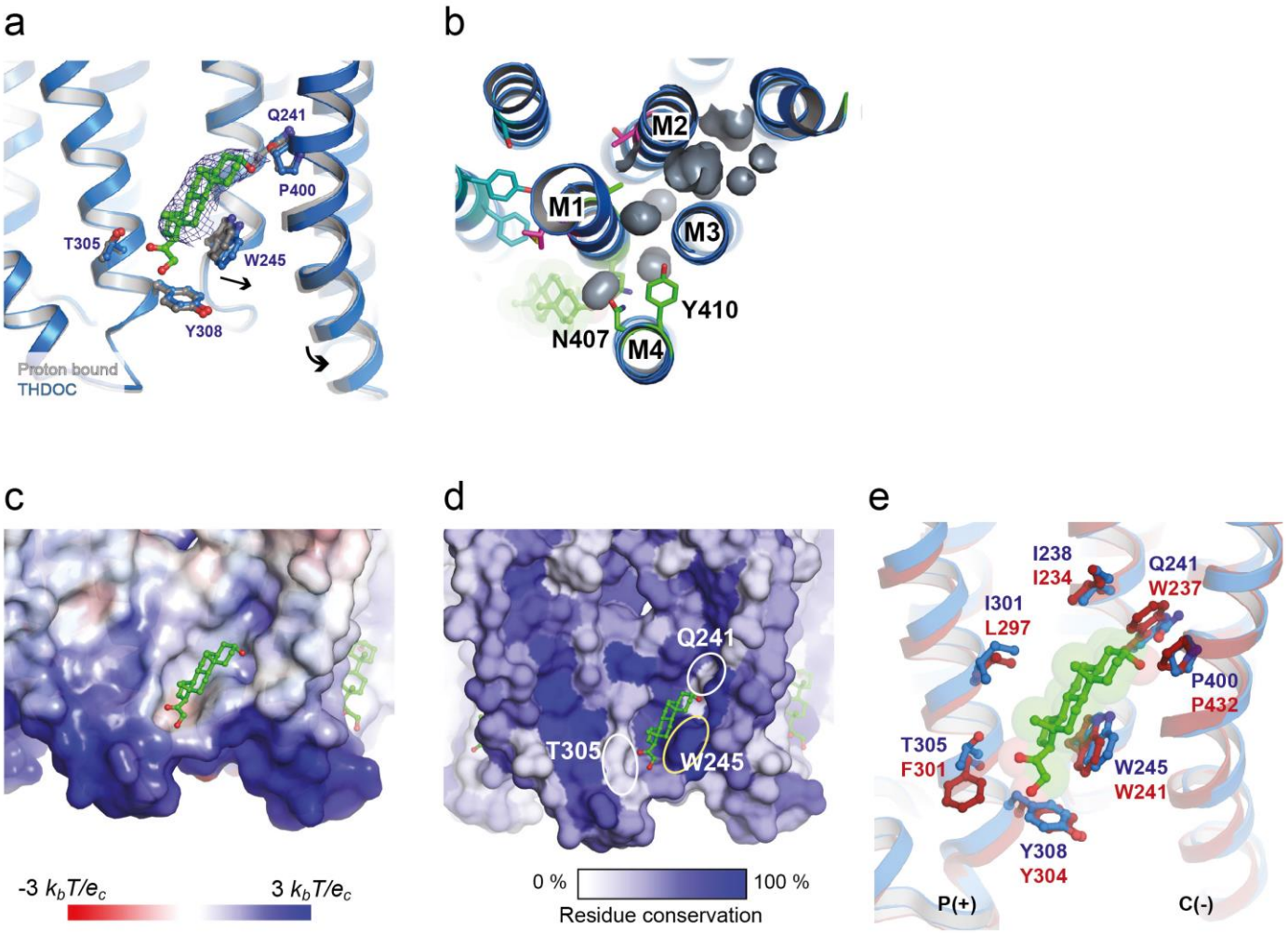


**Supplementary Figure 7**

Defining the binding site for THDOC

(**a**) Superimposition of the proton-bound chimera structure (grey) with THDOC co-crystal structure (dark blue) reveal movement of the TMD. A subtle expansion of the neurosteroid binding pocket is observed to accommodate THDOC, which is more pronounced at the lower end of M4 (arrow). $2F_o$-$F_c$ electron density map (dark blue) contoured at 1.2σ is shown before inclusion of THDOC in refinement. (**b**) Plan view of molecular surface representation of small pockets/cavities (grey) formed within the helical bundle of a single TMD at the level of residues (green, stick representation) previously proposed to form an intra-subunit neurosteroid binding site[14]. (**c**) Electrostatic surface potential at the THDOC binding site (calculated using APBS). Regions of positive and negative charge at either end of the pocket coordinate neurosteroid binding. (**d**) Protein sequence (residue) conservation amongst pLGICs of known structure (as in alignment in Supplementary Fig.1) was mapped onto the structure of the chimera. Notably, for the neurosteroid binding pocket in the $GABA_AR$ α1-subunit, residues at each end that coordinate binding (Q241 and T305) are poorly conserved (white circles), while W245 involved in signal transduction is strongly conserved across pLGICs (yellow circle). (**e**) Superimposition of the GLIC-GABARα1$^{G258V}_{cryst}$ and GABA β3 (PDB ID: 4cof) reveals the nature of the neurosteroid binding site at the β-α interface. Red numbers are equivalent residues contained in β3 subunits.

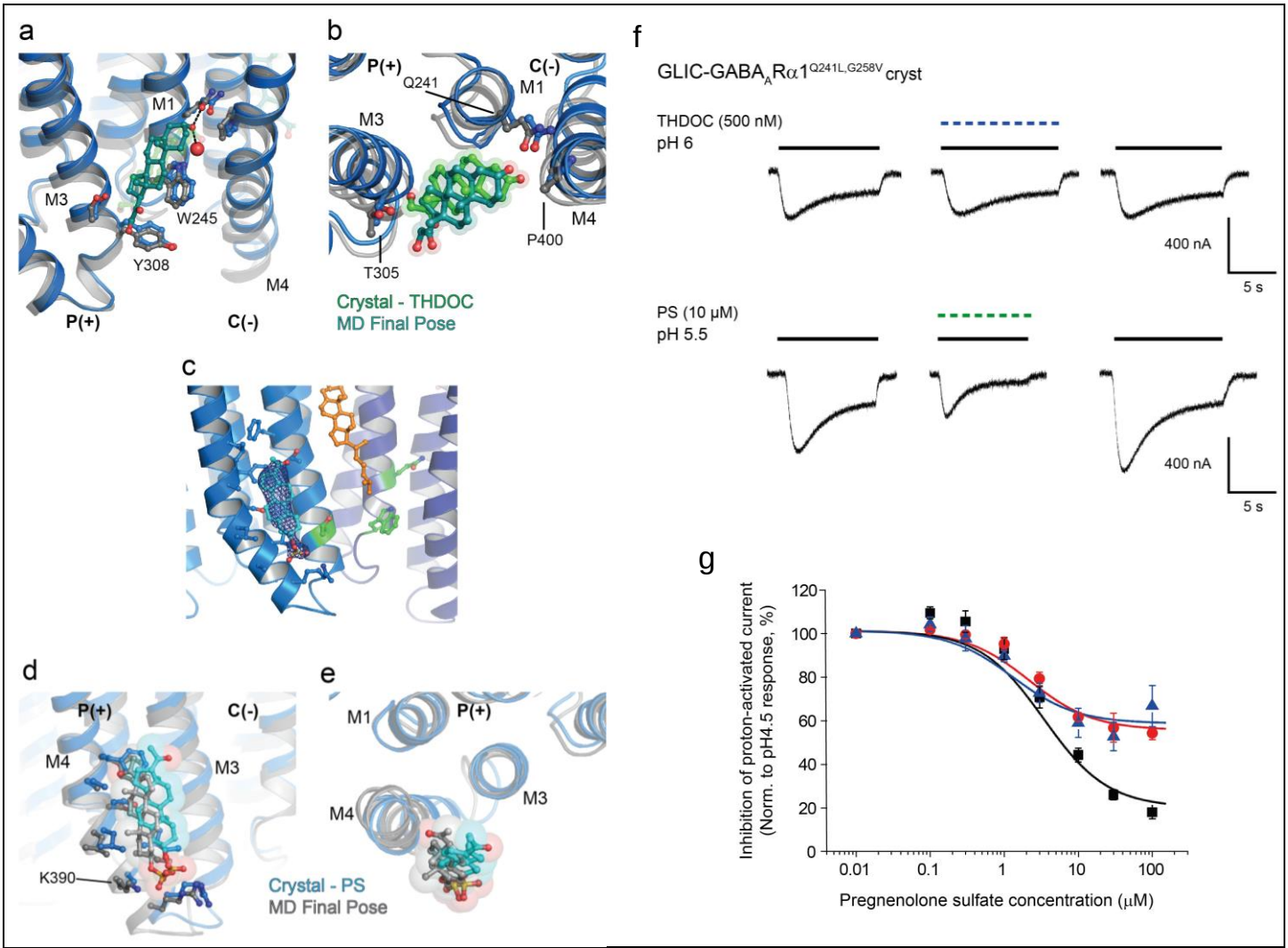


**Supplementary Figure 8**

Molecular dynamics simulations reveal binding poses for THDOC and PS

(**a**) Membrane view of the chimera crystal structure (blue) in complex with THDOC (green sticks) superimposed on the final pose for the chimeric receptor (grey) and THDOC (teal) following molecular dynamics (MD) simulations. (**b**) A plan view from (**a**) reveals the binding site viewed from the extracellular side. (**c**) A membrane view of the TMD for the proton-activated chimera bound with PS (cyan) in the groove created by M3 and M4 α-helices. The image shows a 2Fo-Fc map contoured at 1σ (blue mesh) after refinement of the bound PS molecule. CHS is shown in orange. (**d**) Membrane view of the chimera crystal structure (blue) in complex with PS (cyan sticks and spheres) superimposed on the final pose for the chimeric receptor (grey) and PS (grey sticks and spheres) following MD simulations. During the simulations, PS reaches a stable pose where the β (rough) face of the neurosteroid is exposed to the lipid bilayer. A potential salt bridge is formed between the sulfate group of PS and K390. The side-chain for K390 was disordered in the crystal structure. (**e**) A plan view from (**d**) reveals the binding site and MD pose for PS viewed from the extracellular side. (**f**) Oocytes expressing GLIC-GABA$_A$Rα1$^{G258V}{}_{cryst}$, with the mutation Q241L, are no longer sensitive to the potentiating neurosteroid THDOC, but retain sensitivity to pregnenolone sulfate (PS). Neurosteroids were co-applied (dashed lines) with protons at the indicated pH. The representative currents were replicated 4 and 3 times (for THDOC and PS, respectively). This supports a principal role for Q241 in coordinating the binding of THDOC, and that THDOC and PS binding sites are discrete. (**g**) Theoretical curves for PS inhibition of

GLIC-$GABA_AR\alpha1^{G258V}_{cryst}$ (black line), +K390A (red line) and +I391C, A398C, F399C (blue line), created using the PS kinetic model as described in Supplementary Methods. Experimental data points (colour coded as above for the lines) are taken from Fig. 6e and overlaid on the curves.